

## Weak Lensing Determination of the Mass in Galaxy Halos

D. R. Smith<sup>1,3</sup>, G. M. Bernstein<sup>1</sup>, P. Fischer<sup>4</sup>, & M. Jarvis<sup>1,2</sup>

*Dept. of Astronomy, University of Michigan, Ann Arbor, MI 48109*

deano, garyb, philf, jarvis@astro.lsa.umich.edu

### ABSTRACT

We detect the weak gravitational lensing distortion of 450,000 background galaxies ( $20 < R < 23$ ) by 790 foreground galaxies ( $R < 18$ ) selected from the Las Campanas Redshift Survey (LCRS). This is the first detection of weak lensing by field galaxies of known redshift, and as such permits us to reconstruct the shear profile of the typical field galaxy halo in absolute physical units (modulo  $H_0$ ), and to investigate the dependence of halo mass upon galaxy luminosity. This is also the first galaxy-galaxy lensing study for which the calibration errors due to uncertainty in the background galaxy redshift distribution and the seeing correction are negligible. Within a projected radius of 200  $h^{-1}$  kpc, the shear profile is consistent with an isothermal profile with circular velocity  $v_c = 164 \pm 20$  km s<sup>-1</sup> for an  $L_*$  galaxy, consistent with the typical circular velocity for the disks of spirals at this luminosity. This halo mass normalization, combined with the halo profile derived by Fischer *et al.* (2000) from a galaxy-galaxy lensing analysis of the Sloan Digital Sky Survey, places a lower limit of  $(2.7 \pm 0.6) \times 10^{12} h^{-1} M_\odot$  on the mass of an  $L_*$  galaxy halo, in good agreement with the satellite galaxy studies of Zaritsky *et al.* (1997). Given the known luminosity function of LCRS galaxies, and assumption that  $M \propto L^\beta$  for galaxies, we determine that the mass within  $260 h^{-1}$  kpc of normal galaxies contributes  $\Omega = 0.16 \pm 0.03$  to the density of the Universe (for  $\beta = 1$ ) or  $\Omega = 0.24 \pm 0.06$  for  $\beta = 0.5$ . These lensing data suggest that  $0.6 < \beta < 2.4$  (95% CL), only marginally in agreement with the usual  $\beta \approx 0.5$  Faber-Jackson or Tully-Fisher scaling. This is the most complete direct inventory of the matter content of the Universe to date.

*Subject headings:* gravitational lensing—dark matter—galaxies:halos—galaxies:fundamental parameters—cosmology: observations

---

<sup>1</sup>Visiting Astronomer, National Optical Astronomy Observatories, which is operated by the Association of Universities for Research in Astronomy, Inc., under contract to the National Science Foundation.

<sup>2</sup>Based in part on research carried out at the MDM Observatory, operated by Columbia University, Dartmouth College, University of Michigan, and Ohio State University.

<sup>3</sup>Present Address: Science Dept, Glenelg High School, Glenelg, MD 21737

<sup>4</sup>Present Address: Dept. of Astronomy, Univ. of Toronto, 60 St. George St., Toronto, ON M5S3H8.

## 1. Introduction

Gravitational lensing provides the only non-dynamical measure of the mass distribution of a galaxy halo, and it thus enables a crucial means of quantifying the dark matter halos that are now an essential component of all theories of cosmology and galaxy formation. A reliable measure of the masses of galaxies and their halos also provides a significant lower limit to the density parameter  $\Omega$ . Spiral galaxy halos have traditionally been probed via rotation of stars and gas, but these tracers are not available outside radii of  $\sim 30$  kpc, though their velocities are consistent with an isothermal halo extending beyond this distance. At larger radii, dynamical test particles are scarce: Zaritsky *et al.* (1997) use satellite galaxies to trace the halo mass profile to  $\approx 200$  kpc. Because there are only  $\approx 1.2$  satellites per spiral, the masses of individual galaxies are poorly constrained, but by “stacking” the signals from an ensemble of galaxies, an accurate measure of the mean halo is obtained. A further complication of such dynamical studies of the outer halo is that the test particles are not virialized, and determination of the halo mass requires some model of infall. With such modelling, Zaritsky *et al.* (1997) estimate a mass of  $\sim 2 \times 10^{12} M_{\odot}$  within 200 kpc of an  $L_*$  spiral galaxy.

The gravitational lensing approach uses photons from background galaxies (bggs) as the test particles, enabling halo measurements to large radii. The greatest problem with lensing is the extremely weak shear ( $\lesssim 3\%$ ) associated with the mass of a single galaxy. This is more than a factor of 10 below the noise due to intrinsic shape variations in a single background galaxy. As with the satellite galaxy study, the weak lensing approach must therefore overcome the poor  $S/N$  per galaxy by using large numbers of lens-source pairs, measuring the average galaxy halo. The weak lensing measurement, however, requires no modeling of the dynamical state and can give a non-parametric estimate of the halo profile. The first attempted detection was Tyson *et al.* (1984), and over the last five years several groups have verified the existence of galaxy-galaxy lensing based upon analysis of a small number of deep fields (Brainerd, Blandford, & Smail 1996; Dell’Antonio & Tyson 1996; Griffiths, Casertano, & Ratnatunga 1996; Hudson *et al.* 1998). Interpretation of these results is problematic not only because of poor  $S/N$ , but also because the redshifts of the lens galaxies (and hence their distances and luminosities) are not known individually. Interpretation relies upon positing a model for the joint distance/luminosity distribution of the lenses and sources, and a model for dependence of halo mass and size upon luminosity, then projecting these models down to a function of angular variables to be compared with the observations. In such deep fields, even the statistical distributions of lens and source distances are currently ill-determined.

More recently Fischer *et al.* (2000, F00) have measured a galaxy-galaxy lensing signal at high significance from preliminary Sloan Digital Sky Survey data. These data are relatively shallow (foreground galaxies  $16 < r' < 18$ , background galaxies  $18 < r' < 22$ ), which weakens the shear signal, but this is more than compensated by the extremely large sample size of  $\approx 16$  million fgg/bgg pairs. These data indicate that halos of typical galaxies continue an isothermal profile to a radius of at least  $260 h^{-1}$  kpc. The conversion from shear amplitude to mass density in the F00 data is still reliant upon photometric redshift distributions for the fggs and bggs.

We present here a detection of galaxy-galaxy lensing around fggs with redshifts determined by the Las Campanas Redshift Survey (Shectman *et al.* 1996) We thus have knowledge of the fgg luminosity and distance, and the impact parameter of the lensed photons, in physical units (*i.e.* kpc rather than arcsec), information that is normally lost in projection. The bgg’s ( $R < 23$ ) are at magnitudes within the reach of current pencil-beam redshift surveys, and hence their distance distribution is well enough determined to introduce negligible uncertainty in the calibration. We are therefore in theory able to measure the galaxy luminosity  $L$ , halo mass  $M$ , and surface mass density  $\Sigma$  in physical units without ambiguity (save the scale factor  $H_0$ ). In practice our  $S/N$  is too low to constrain the extent of the galaxy halo meaningfully, so we combine the F00 profile *shape* with our *normalization* to obtain a mass profile in absolute units. Combining the resultant  $M/L$  with the well-determined luminosity function of the LCRS galaxies (Lin *et al.* 1996) we obtain the galactic contribution to  $\Omega$ . We assume an Einstein-deSitter Universe for the values presented here, and use  $H_0 = 100h \text{ km s}^{-1} \text{ Mpc}^{-1}$ . Because the fggs are relatively nearby, and the bggs are far behind them, the dependence of the results upon the cosmological parameters  $\Omega$  and  $\Lambda$  is negligible ( $< 2\%$ ).

## 2. Observations and Reduction Methods

### 2.1. Observations

We observed 36 square degrees of sky in  $R$  band using the Big Throughput Camera (BTC) (Wittman *et al.* 1998) on the CTIO Blanco 4-meter telescope over three runs from December 1996 through March 1999. Most areas of the target fields are covered by three dithered 420-second exposures. Observations were made within the Las Campanas Redshift Survey fields and yield  $\approx 45,000$  well-measured bggs per  $\text{deg}^2$ , with typical seeing of  $1''.1$  FWHM and RMS sky noise of  $\approx 28 R \text{ mag arcsec}^{-2}$  on  $0''.43$  pixels. Images are debiased and flattened using standard IRAF<sup>5</sup> routines. Rather than sum images, we analyze each 300s exposure separately and average the resulting galaxy measurements. This allows us to adjust for exposure-to-exposure seeing variations as well as to avoid or isolate various systematic errors. Observations of  $R$ -band standards from Landolt (1992) yield photometric solutions with worst-case RMS errors of 0.05 mag.

### 2.2. Shape Measurement

Galaxy shape measurements are critical to weak lensing. Detailed descriptions of our methods are presented in Bernstein *et al.* (2000) and Smith (2000). Here we summarize the processing steps.

---

<sup>5</sup>IRAF is distributed by the National Optical Astronomy Observatories, which is operated by the Association of Universities for Research in Astronomy, Inc. (AURA) under cooperative agreement with the National Science Foundation.

Initial detection, photometry, and size estimation is done by `SExtractor` (Bertin & Arnouts 1996). This information is then fed to our shape measurement code `elliptomatic`, which determines ellipticities from Gaussian-weighted second moments of each object. The Gaussian weights are elliptical; the weight ellipticity is iterated to match the object’s ellipticity, which produces an unbiased estimate of the object shape. Stellar objects are selected from the catalog, and a position-dependent convolution kernel is created which, when applied to the original image, makes the stellar PSF round everywhere in the image (Fischer & Tyson 1997; Bernstein *et al.* 2000) This corrects all objects for shape errors induced by telescope tracking, seeing, or linear CCD charge transfer inefficiencies. Optical distortions are significant across the wide field of the BTC. Observations of astrometric standard fields yield a distortion map, and object shapes are corrected for this distortion analytically, yielding the observed (post-seeing) ellipticity components  $e_1^o$  and  $e_2^o$ . The observed shapes are then corrected for the circularizing effects of the PSF to give an estimate of the pre-seeing ellipticity  $e_1^i$  and  $e_2^i$  which would be observed in an image with perfect resolution. If this correction is larger than a factor of 5, the object is discarded. The measured ellipticities of a given object on different exposures are averaged to give the mean pre-seeing ellipticity for that object. An estimated uncertainty  $\sigma_e$  due to image noise is also calculated for each object.

When considering the distortion induced by a given fgg, the bgg ellipticity is rotated to components  $e_+$  and  $e_x$ , where the former is positive for an image oriented tangentially to the fgg.

The algorithms used herein to correct for PSF anisotropy and circularization are known to leave systematic residuals at the  $\sim 0.5\%$  level in the shapes of the galaxies. These have little effect upon the galaxy-galaxy lensing measurements since one is measuring  $\langle e_+ \rangle$  in annuli about the fgg, and a systematic distortion of constant orientation will cancel to first order when integrated around the annulus. We will demonstrate the absence of significant systematic errors below.

### 2.3. Determination of Distortion from Ellipticities

A given bgg with source-plane tangential ellipticity  $e_+^s$ , when subjected to a weak (tangential) distortion  $\delta$ , will in the absence of noise be measured to have image-plane ellipticity

$$e_+^i = e_+^s + \delta[1 - (e_+^s)^2]. \quad (1)$$

Since the bgg orientations are assumed isotropic,  $\langle e_+^s \rangle_b = 0$ , a useful unbiased estimator for the distortion is

$$\hat{\delta} = \langle e_+^i \rangle_b / \mathcal{R}, \quad \mathcal{R} \equiv \langle 1 - (e_+^i)^2 \rangle_b \equiv 1 - \sigma_{SN}^2, \quad (2)$$

where  $\sigma_{SN}^2 \equiv \langle (e_+^i)^2 \rangle_b$  is often called the *shape noise*. The *responsivity*  $\mathcal{R}$  is similar to the mean “shear polarizability” of Kaiser, Squires, & Broadhurst (1995). In the presence of measurement error  $\sigma_e$  upon each ellipticity, we may wish to apply some weight function  $w(e, \sigma_e)$  to each bgg shape. The estimator for local distortion becomes (Bernstein *et al.* 2000)

$$\hat{\delta} = \frac{1}{\mathcal{R}} \frac{\sum_b w e_+^i}{\sum_b w} \quad (3)$$

$$\mathcal{R} \equiv \frac{\sum_b \left[ w(1 - fe_+^2) + \frac{\partial w}{\partial e} \frac{e_+^2}{e} (1 - fe^2) \right]}{\sum_b w} \quad (4)$$

$$f \equiv \frac{\sigma_{SN}^2}{\sigma_{SN}^2 + \sigma_e^2}. \quad (5)$$

The parameter  $f$  describes the fraction of the variance in measured  $e_+^i$  for the bgg population which is attributable to shape noise. Any weight function is permissible if it depends only upon the magnitude, not the direction, of the ellipticity  $e$ . We use the following weight, which can be shown to minimize the variance of the estimator under certain conditions (Bernstein *et al.* 2000):

$$w(e, \sigma_e) = \frac{1 - (fe^o)^2 + \sigma_{SN}^2(4f - 1)}{\sigma_{SN}^2 + \sigma_e^2}. \quad (6)$$

Alternative choices of weight function lead to results that are indistinguishable within the noise.

We have tested the accuracy of the distortion-measurement algorithms using simulated data frames. An image of artificial spiral and elliptical galaxies is distorted by a circular isothermal potential, then subjected to degradation by Gaussian seeing and noise similar to those in our images. The artificial images are then run through the software pipeline, and the above equations used to extract the distortion  $\delta$  as a function of radius from the putative lens. The results are plotted in Figure 1, which illustrates that the input distortion is recovered to an accuracy of 5% or better as long as the distortion is indeed weak. To insure that the calibration of PSF circularization is correct and robust, we repeat the simulation with the angular sizes of the bgg's arbitrarily reduced by 30%. The input distortion is again recovered to the same accuracy.

An additional complication of the real data is that the bgg's are distributed in redshift but the distances to individual galaxies are not known. Pencil-beam redshift surveys give the joint distribution  $N(m, z)$  of the background population. We will assume that the responsivity  $\mathcal{R}$  and weight  $w$  of the bgg's are uncorrelated with bgg redshift  $z_b$  at a given bgg magnitude  $m_b$ . Then the  $\hat{\delta}$  quantity in Equation (3) is a scaled estimator of the distortion  $\delta_\infty$  that would be measured for a bgg population at infinite redshift:

$$\langle \hat{\delta} \rangle = \delta_\infty \frac{\sum_b w \bar{F}_D(z_f, m_b)}{\sum_b w} \quad (7)$$

$$\bar{F}_D(z_f, m_b) = \frac{\int_{z_f}^{\infty} (D_{fb}/D_{ob}) N(m_b, z_b) dz_b}{\int_0^{\infty} N(m_b, z_b) dz_b}. \quad (8)$$

The  $D$ 's are angular diameter distances between observer, foreground, and background redshifts. The quantity  $\delta_\infty$  is thus measurable as long as the distribution of the background weight vs redshift is known. The redshift distribution of our bgg sample is sufficiently well known from deep redshift surveys that the uncertainty in the factor  $\bar{F}_D$  does not dominate the error budget, as will be discussed in detail below.

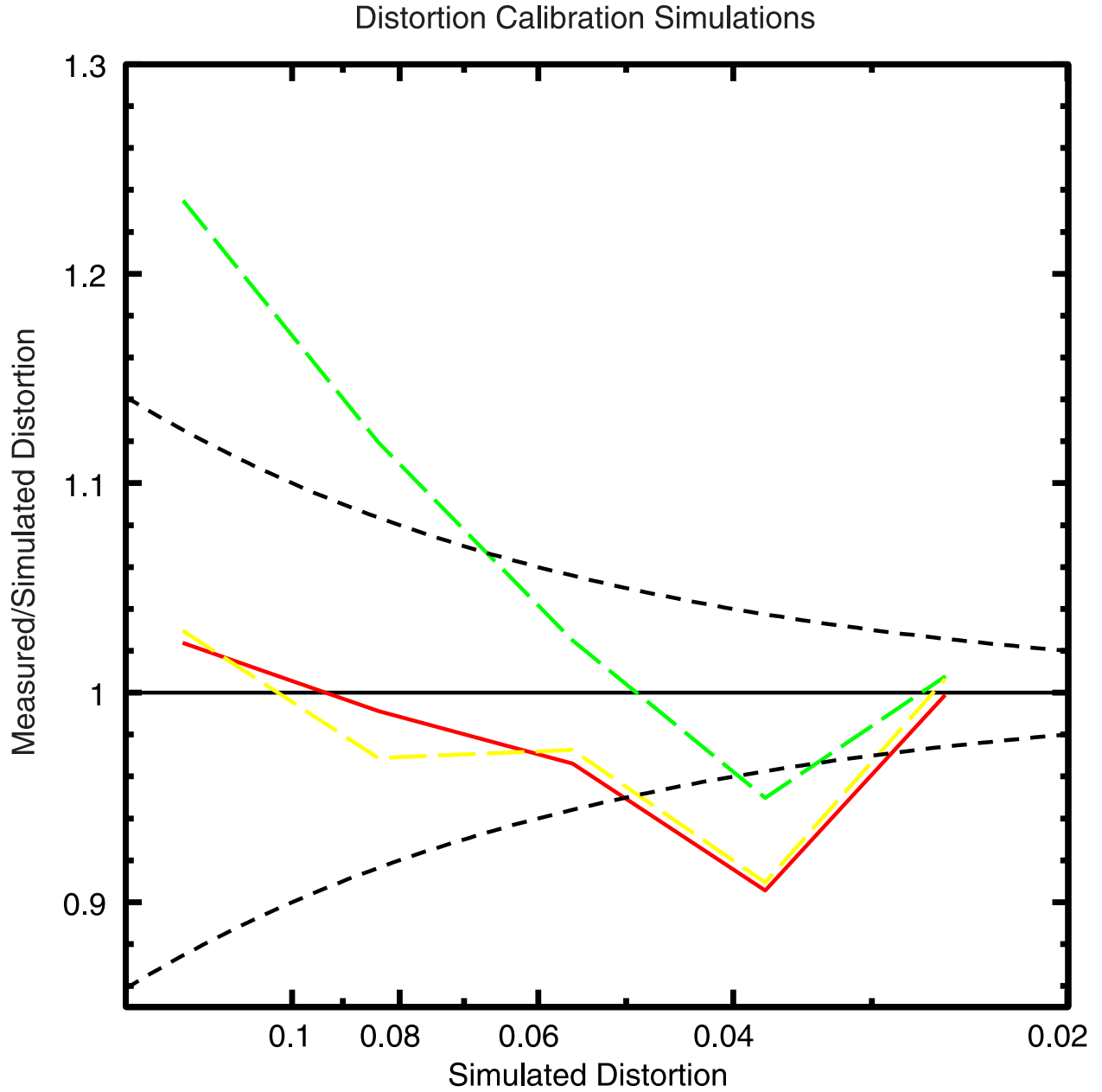


Fig. 1.— Results of shear calibration with simulated data: a simulated isothermal distortion is applied to artificial galaxy images, which are then measured via the standard measurement pipeline. The ratio of the measured to the applied distortion is shown for our standard weighting scheme (solid line) and two alternative weighting schemes (dashed lines). Ideally the ratio is unity to order  $e$ , *i.e.* will fall between the two dashed curves. The measured values are within  $\sim 5\%$  of the applied distortion in the limit of weak lensing, and are nearly independent of weighting scheme. The results are not visibly changed when the artificial galaxy sizes are reduced by 30%.

## 2.4. Mass Density and Scaled Distortion

The physical quantity of interest is the mean azimuthally averaged surface mass density  $\Sigma_L(R)$  at radius  $R$  about galaxies of luminosity  $L$ . The measured quantity is the lensing distortion  $\delta_\infty$  induced upon a distant bgg  $z_b$ , which is related to the surface density by

$$\delta_\infty(R, L, z_f) = [\Sigma_L(\leq R) - \Sigma_L(R)] \frac{8\pi G}{c^2} D_{of} \quad (9)$$

Here  $\Sigma_L(\leq R)$  is the average surface mass density interior to  $R$ . We will wish to combine data from fggs which span a range of  $z_f$ , and we additionally will bin data over finite ranges in impact parameter  $R$ , and fgg luminosity  $L$ . To compensate for the spread in these quantities, we express the distortion  $\delta_\infty(R, L, z_f)$  for a given fg/bg pair in terms of a scaled distortion

$$\delta_* \equiv \delta(R = R_0, L = L_*, z_f = z_*, z_b = \infty) \quad (10)$$

$$= \delta_\infty(R, L, z_f) / [F_L(L)F_R(R)F_z(z_f)]. \quad (11)$$

Our canonical luminosity is the  $L_*$  in the Schechter-function parameterization of the LCRS galaxy luminosity function, which is absolute  $R$ -band magnitude  $M_* = -20.3 + 5 \log h$ , or  $L_* = 8.4h^{-2} \times 10^9 L_\odot$  (Lin *et al.* 1996)  $z_*$  is taken to be 0.1, the median redshift of the LCRS sample; and  $R_0$  is taken as  $100h^{-1}$  kpc if not otherwise specified as the center of some radial bin. The scaling factor for redshift is known:

$$F_z(z_f) = D_{of}(z_f) / D_{of}(z_*) \quad (12)$$

Scaling the measured shear to a standard luminosity and radius requires some model for how the surface density profile varies with these quantities. With a sufficiently large galaxy sample, one could simply measure the function  $\Sigma_L(\leq R) - \Sigma_L(R)$  in narrow bins of  $L$  and  $R$ , and non-parametrically map this density contrast as a function of these two variables. Our samples are, however, small enough that our bins must cover a substantial range of  $L$  and  $R$ , so we will adopt the assumption that the surface density is described by an isothermal profile with a circular velocity  $v_c$  that is a power-law function of luminosity:

$$\Sigma_L(R) = \Sigma_L(\leq R) / 2 = \frac{v_c^2(L)}{4GR}, \quad v_c(L) = v_*(L/L_*)^{\beta/2}. \quad (13)$$

The scaling functions are then very simple:

$$F_L = (L/L_*)^\beta, \quad F_R = R_0/R. \quad (14)$$

The canonical distortion is

$$\delta_* = 2\pi \frac{v_*^2}{c^2} \frac{D_{of}(z_*)}{R_0} = 0.0071 \left( \frac{v_*}{200 \text{ km s}^{-1}} \right)^2 \left( \frac{R_0}{100h^{-1} \text{ kpc}} \right)^{-1} \quad (15)$$

The high-S/N data of F00 produce a mean distortion profile that is fully consistent with the isothermal profile at the radii  $R \lesssim 200h^{-1}$  kpc in which we measure  $\delta$ . The power-law dependence

of  $\Sigma$  upon galaxy luminosity  $L$  is suggested by the Tully-Fisher and Faber-Jackson relations, which lead us to choose the value  $\beta = 0.5$ . These relations have, however, been tested only at radii of  $\sim 30h^{-1}$  kpc or smaller—the F00 study cannot test this since the fgg luminosities are not known individually. Indeed Zaritsky *et al.* (1997) were unable to detect *any* dependence of halo mass upon luminosity in the spiral satellite study. We will also calculate  $\delta_*$  under the assumption  $\beta = 1$ , the mass-traces-light value. In §3.5 we will use our own data to bound  $\beta$ .

The goal of this paper is an absolute determination of  $\delta_*$ . Our estimator for  $\delta_*$  combines Equations (3), (7), and (10). In addition the variance of the estimator is minimized by adding a factor of  $(F_L F_R F_z \bar{F}_D)^2$  to the weight function. We thus obtain

$$\hat{\delta}_* = \frac{1 \sum_{f,b} w F_L F_R F_z \bar{F}_D e_+^i}{\mathcal{R} \sum_{f,b} w [F_L F_R F_z \bar{F}_D]^2} \quad (16)$$

Standard propagation of errors, along with the substitution  $\text{Var}(e_+) = \langle e_+^2 \rangle$ , yields the variance of the above estimate:

$$\text{Var}(\hat{\delta}_*) = \frac{\sum_{f,b} [w F_L F_R F_z \bar{F}_D e_+^i]^2}{\mathcal{R}^2 \left\{ \sum_{f,b} w [F_L F_R F_z \bar{F}_D]^2 \right\}^2} \quad (17)$$

### 3. Results

Our foreground sample consists of all 790 galaxies from the LCRS redshift survey with  $0.05 < z_f < 0.167$  that lie within our imaged areas. Background galaxies are required to be well-measured on at least two exposures, have magnitude  $20 < R < 23$ , and correction for PSF circularization at most a factor 5 (this is effectively a lower limit on angular size). This leaves  $\approx 450,000$  fgg/bgg pairs with impact parameters of  $15h^{-1} \text{ kpc} \leq R \leq 480h^{-1} \text{ kpc}$ .

#### 3.1. Background Galaxy Redshift Distribution

An absolute determination of mass densities requires an estimate of the distance factor  $\bar{F}_D(z_f, m_b)$  from the weighted redshift distribution of the background galaxies. The Caltech Redshift Survey of the Hubble Deep Field and its flanking fields (Cohen *et al.* 2000, CRS) provides a virtually complete redshift survey to  $R \leq 23$ . We combine the CRS  $N(m, z)$  data into 0.5-mag bins to construct the function  $\bar{F}_D$ . This factor is above 0.6 for nearly all the fgg/bgg pairs in our data, and is by definition  $\leq 1$ . This limited range of variation is a consequence of the substantial magnitude (hence distance) gap between our foreground and background samples, and makes our calibration very stable against perturbations in the assumed  $N(m, z)$ . Thus while the HDF field may be deficient in nearby galaxies, we do not expect a significant effect upon our results.

To estimate the uncertainty in  $\delta_*$  due to  $\bar{F}_D$  errors we turn to the Canada-France Redshift Survey (Crampton *et al.* 1995, CFRS), which is nearly complete for a sample of  $\approx 600$  galaxies in

5 fields defined by  $I_{AB} < 22.5$ . We have imaged two of these fields in  $R$  band using the 2.4-meter Hiltner telescope at MDM Observatory to obtain an  $N(m_R, z)$  distribution of the CFRS sample. We can either use the measured  $N(m_R, z)$  in these two fields, or use them to construct a mean  $(R - I_{AB})$  vs  $(V_{AB} - I_{AB})$  color relation for the galaxies, and apply this relation to the full CFRS catalog to mimic an  $R$ -band observation. The values of  $\delta_*$  determined by the two methods differ by only  $\approx 1\%$ .

Using the measured CFRS  $N(m, z)$  changes  $\delta_*$  by  $\pm 5\%$  or less relative to the use of the CRS. The CFRS is substantially incomplete in two senses: first, the  $I_{AB} < 22.5$  cutoff of the CFRS catalog misses an unknown number of the bluer  $R < 23$  galaxies. These bluer galaxies are likely nearer, on average, than the measured  $R \approx 23$  sample. Second, the CFRS redshift measurements are incomplete even for the  $I_{AB} < 22.5$  sample; this incompleteness is as large as 30% in the  $22.5 < R < 23.0$  bin. These galaxies are likely to be biased toward the  $1 < z < 2$  range where redshift measurement is difficult. If we place all the unmeasured galaxies at  $z = 2$ ,  $\delta_*$  is still only 6% lower than the CRS result—and it is likely that inclusion of the missing blue  $R \approx 23$  galaxies would push this number back toward the CRS result.

We conclude that calibration errors due to uncertainties in the bgg redshifts are  $< 5\%$ .

### 3.2. Measured Halo Properties

We plot the scaled distortion  $\delta_*$  as a function of proper distance from the lens galaxy center in Figure 2. The tangential alignment is clearly detected to  $\sim 150h^{-1}$  kpc. As a test for systematic contamination, we calculate the azimuthal average of  $e_\times$ . The  $e_\times$  averages are consistent with zero distortion, as they must be if the distortion is due to weak lensing (Stebbins, McKay, & Frieman 1996), giving us confidence that systematic shape distortions have minimal effect upon our  $\delta_*$  determination.

Our data are consistent with an isothermal profile but are too noisy to provide any useful constraint on the profile shape. No useful lower limit, for example, is implied upon a possible outer truncation radius  $R_{\max}$  for an isothermal halo. The high-S/N data of F00, however, do provide useful constraints to the truncation radius which we will use below.

The most accurate determination of  $\delta_*$  is made by fitting all the data with  $15h^{-1}$  kpc  $< R < 240h^{-1}$  kpc to the isothermal model. For the two trial values of  $\beta$  we obtain

$$\delta_* = \begin{cases} 0.0056 \pm 0.0014 & \beta = 0.5 \\ 0.0048 \pm 0.0010 & \beta = 1.0 \end{cases} \quad (18)$$

In either redshift model the lensing signal is detected at signal-to-noise ratio of 4–5. For comparison, the  $\delta_\times$  values computed over this broad bin are  $(1. \pm 11) \times 10^{-4}$  ( $\beta = 1$ ), consistent with zero within the calculated uncertainties.

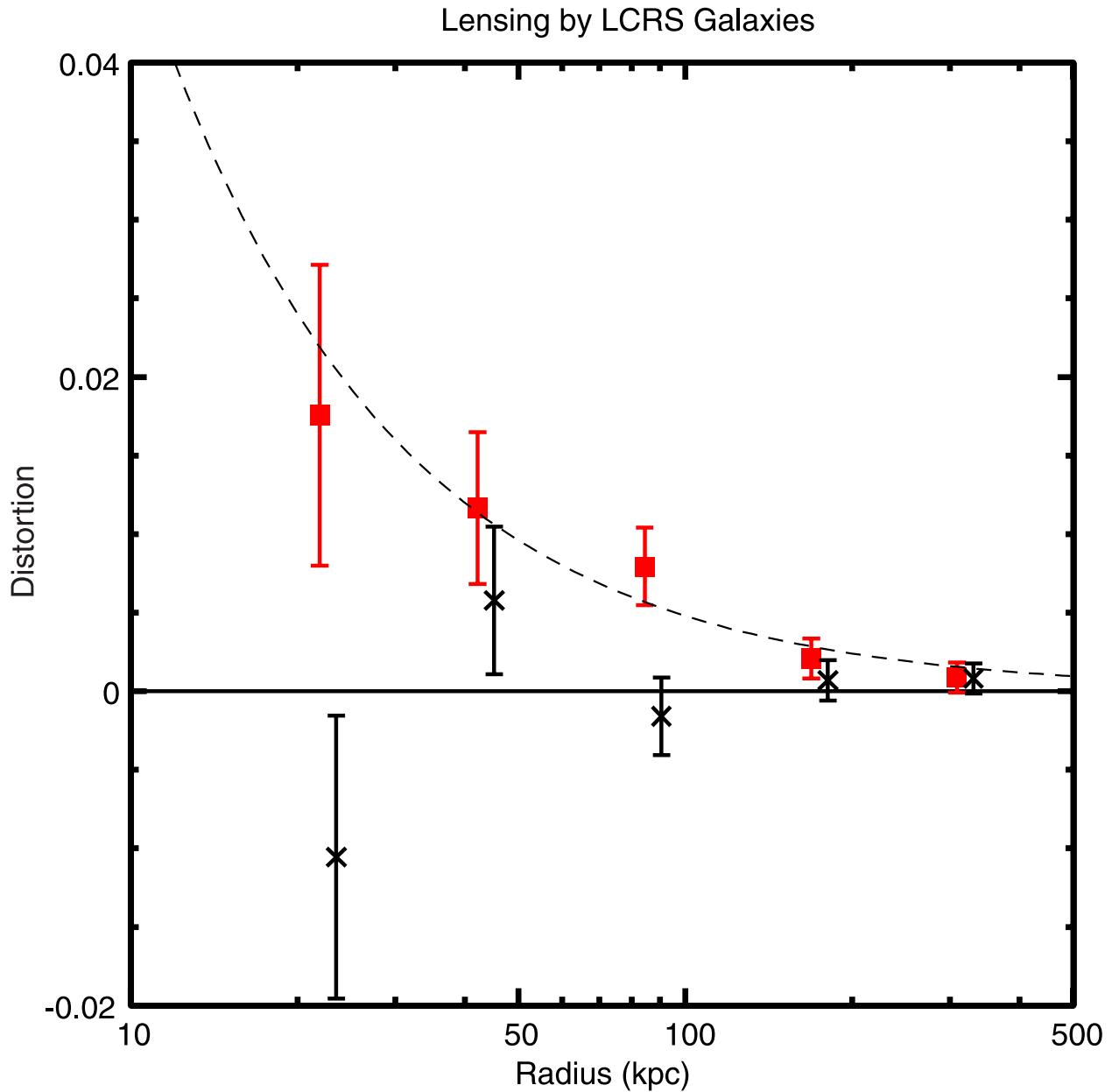


Fig. 2.— The square symbols show the measured distortion  $\delta_*$  (scaled to an  $L_*$  galaxy at  $z_f = 0.1$  and  $z_b = \infty$ ) vs impact parameter. The dashed line is the best-fit isothermal model. The cross symbols ( $\times$ ) show the binned means of the  $\delta_\times$  component of shear, which should (and does) vanish if the distortions are due entirely to lensing. This plot depicts results assuming  $M \propto L^\beta$  with  $\beta = 1$ , and the total significance of the detection is  $4.5\sigma$ . The results for  $\beta = 0.5$  are similar.

### 3.3. Sources of Error

Possible sources of error in our determination of  $\delta_*$  include:

1. *Noise*: the largest source of error is the random shape noise and measurement noise in the ellipticities of the bggs. This contributes an uncertainty of 20–25% ( $1\sigma$ ) to  $\delta_*$ , and is the error quoted in Equation (18).
2. *Background Redshifts*: As discussed above, the  $R < 23$  redshift distribution is known well enough to reduce calibration uncertainty to  $\pm 5\%$  or less.
3. *Distortion Calibration*: The accuracy with which our software measures the galaxy shapes, corrects to the pre-seeing shapes, and calculates a distortion has been tested by the simulations. This accuracy appears to be  $\approx 5\%$  or better.
4. *Mis-measurement*: One could imagine that the shape measurements of background galaxies could be biased by the wings of the foreground galaxies. At radii beyond  $30h^{-1}$  kpc, however, the light from the foreground galaxies is far below the noise of the images.
5. *Luminosity Scaling*: The measured  $\delta_*$  depends to some degree on the index  $\beta$  scaling luminosity to mass [Equation (13)]. We will attempt to measure  $\beta$  below.
6. *Satellite Galaxies*: Our sample of “background galaxies” will be diluted by faint galaxies that are physically associated with the foreground galaxies.  $\delta_*$  should be adjusted upward by a factor equal to the fraction of bgg’s that are in fact satellite galaxies. F00 measure this contamination to be about 15% at a projected radius of  $\sim 60h^{-1}$  kpc, where our data are centered. Our fgg sample is similar to that of F00, but the bgg magnitude ranges differ:  $18 < r' < 22$  for F00, and  $20 < R < 23$  for us. Our fainter bgg sample should have a substantially smaller fraction of physically associated galaxies since background counts rise much more quickly (factor of 2.5 per magnitude in  $R$ , (Tyson 1988)) than the dwarf galaxy luminosity function (factor of 1–1.5 per mag). We detect this effect in our own data, but it is difficult to measure precisely. We estimate, however, that our contamination factor should be below the 10% level.
7. *Projected Neighbors*: The distortion  $\delta(R)$  measures the surface mass density (above the cosmic mean density) projected within radius  $R$  of a fgg. As galaxies are clustered in space, a circle of radius  $R$  about a fgg actually includes mass from the halos of excess neighboring galaxies. The strength of this effect can be estimated by convolving the galaxy-galaxy correlation function  $\xi(r) \approx (r/8h^{-1}\text{Mpc})^{-1.8}$  with an isothermal mass distribution. At our radii of  $R \sim 100h^{-1}$  kpc the effect is quite small ( $\approx 4\%$ ) and can be ignored. Beyond  $200h^{-1}$  kpc the effect rises above 10% and must be taken into account (see F00). Note that this effect opposes that of satellite “dilution” mentioned previously, but both tend to flatten the run of  $\delta$  with radius.

In summary, the errors in  $\delta_*$  are dominated by random noise at  $\pm 20\%$ . There are 4 calibration uncertainties each at  $\lesssim 5\%$  level, which are known to work in dissimilar directions, so the overall calibration uncertainty should be below 10% (save the uncertainty in  $\beta$ ), and will be ignored.

### 3.4. Total Mass in Galaxy Halos

The halo mass profiles are consistent with an isothermal profile to the  $\sim 200h^{-1}$  kpc radii we probe; the total mass associated with each galaxy depends upon the extent of these isothermal halos. If the surface density of a galaxy follows the isothermal profile in Equation (13) to a projected radius  $R_{\max}$ , beyond which it is abruptly truncated, then the total mass of a typical galaxy at luminosity  $L$  is

$$M(L) = M_*(L/L_*)^\beta, \quad (19)$$

$$M_* = \frac{\pi}{2G} v_*^2 R_{\max} \quad (20)$$

$$= 2.06 \times 10^{14} h^{-1} M_\odot \delta_* \left( \frac{R_{\max}}{100h^{-1} \text{ kpc}} \right). \quad (21)$$

Our data do not constrain  $R_{\max}$ , so we turn to the SDSS data. The F00 distortions are fit to a model in which all galaxies are truncated at some angular size  $s$ ; F00 obtain a 95% CL lower limit of  $s > 140''$  for their sample.<sup>6</sup> The estimated redshift distribution of fggs in the F00 sample has a weighted mean angular diameter distance of  $0.125c/H_0$ , so a simple estimate of the physical scale of the truncation radius is  $s > 260h^{-1}$  kpc at 95% CL. The F00 model ignores possible variations of halo extent with galaxy luminosity, but such considerations are not likely to influence our result because the mass integrals and the F00 data are both dominated by galaxies near  $L_*$ . We will therefore adopt from F00 the result

$$R_{\max} \geq 260h^{-1} \text{ kpc} \quad (95\% \text{ CL}). \quad (22)$$

Taken with Equations (18) and (21), this implies that the total mass and mass-to-light ratio for an  $L_*$  galaxy contained within projected radius of  $260h^{-1}$  kpc are:

$$M(< 260h^{-1} \text{ kpc}) = \begin{cases} (3.1 \pm 0.8) \times 10^{12} h^{-1} M_\odot & (\beta = 0.5) \\ (2.7 \pm 0.6) \times 10^{12} h^{-1} M_\odot & (\beta = 1.0) \end{cases} \quad (23)$$

$$M(< 260h^{-1} \text{ kpc})/L = \begin{cases} (360 \pm 90)h M_\odot/L_{\odot,R} & (\beta = 0.5) \\ (310 \pm 60)h M_\odot/L_{\odot,R} & (\beta = 1.0) \end{cases} \quad (24)$$

Note that the LCRS luminosities are isophotal, and Lin *et al.* (1996) recommend raising the luminosity estimates (hence lowering  $M/L$ ) to account for flux excluded from the apertures. There has also been no account taken of evolution since  $z \sim 0.1$ , though a  $K$ -correction is made.

---

<sup>6</sup>The fitting function in F00 is not quite a cylindrical truncation at  $s$ , but the integrated mass is the same.

Using the Schechter-function parametric fit to the LCRS galaxy luminosity function from (Lin *et al.* 1996) and the mass formula in Equation (19), the mean mass density in galaxy halos is  $M_*\phi_*\Gamma(1 + \alpha + \beta)$ , where  $\phi_* = 0.019h^3\text{Mpc}^{-3}$  and  $\alpha = -0.70$  are the fitted Schechter-function parameters. As a fraction of the critical density, the density in LCRS halos is

$$\Omega_{\text{halo}} = \begin{cases} 16.4 \delta_* \left( \frac{R_{\text{max}}}{100h^{-1} \text{ kpc}} \right) \geq 0.23 \pm 0.06 & (\beta = 0.5) \\ 12.7 \delta_* \left( \frac{R_{\text{max}}}{100h^{-1} \text{ kpc}} \right) \geq 0.16 \pm 0.03 & (\beta = 1.0) \end{cases} \quad (25)$$

These constitute a lower limit to  $\Omega$  since the matter associated with galaxies may well extend beyond  $260h^{-1}$  kpc. Furthermore we have only inventoried matter which is associated with galaxies included in the LCRS sample. Low-surface-brightness galaxies excluded from the LCRS would increase  $\Omega$  to some extent, as of course would any form of matter which is not spatially correlated with the centers of LCRS galaxies.

### 3.5. Mass vs Luminosity

The largest uncertainty in our calculation of  $\Omega$  is the exponent  $\beta$  describing dependence of galaxy mass upon luminosity. This parameter is normally assumed to be near 0.5 based upon dynamical measures in the luminous parts of galaxies, but it is purely an ansatz for mass at radii beyond  $30h^{-1}$  kpc. We have divided our foreground sample into 3 bins of luminosity and fit an isothermal distortion profile to an annulus  $15h^{-1} \text{ kpc} < R < 240h^{-1} \text{ kpc}$  for each bin. In Figure 3 the dependence of distortion (mass) upon  $L$  is readily apparent. This is in contrast to the Zaritsky *et al.* (1997) satellite galaxy study, which did not see a significant correlation between luminosity and halo mass at  $200h^{-1}$  kpc. The galaxies certainly “know” about the density of the halos in which they are embedded.

The dependence of  $\delta$  upon  $L$  is readily fit by the Equations (13) for the mass-traces-light value of  $\beta = 1$ , ( $\chi^2/\nu = 1.16/2$ ). The Faber-Jackson value of  $\beta = 0.5$  is somewhat disfavored ( $\chi^2/\nu = 4.93/2$ ,  $Q = 0.09$ ). Treating  $\beta$  as a free parameter in a fit to the three bins yields a 95% CL range of  $0.6 < \beta < 2.4$ . This result is intriguing and demonstrates the power of weak lensing to elucidate the relation between luminous and dark matter. The traditional  $\beta = 0.5$  model is not strongly excluded, however, so we will await further data before drawing conclusions.

A similar marginal difference is seen between the masses of absorption-spectrum and emission-spectrum galaxies in the foreground sample, but meaningful results must await better statistics.

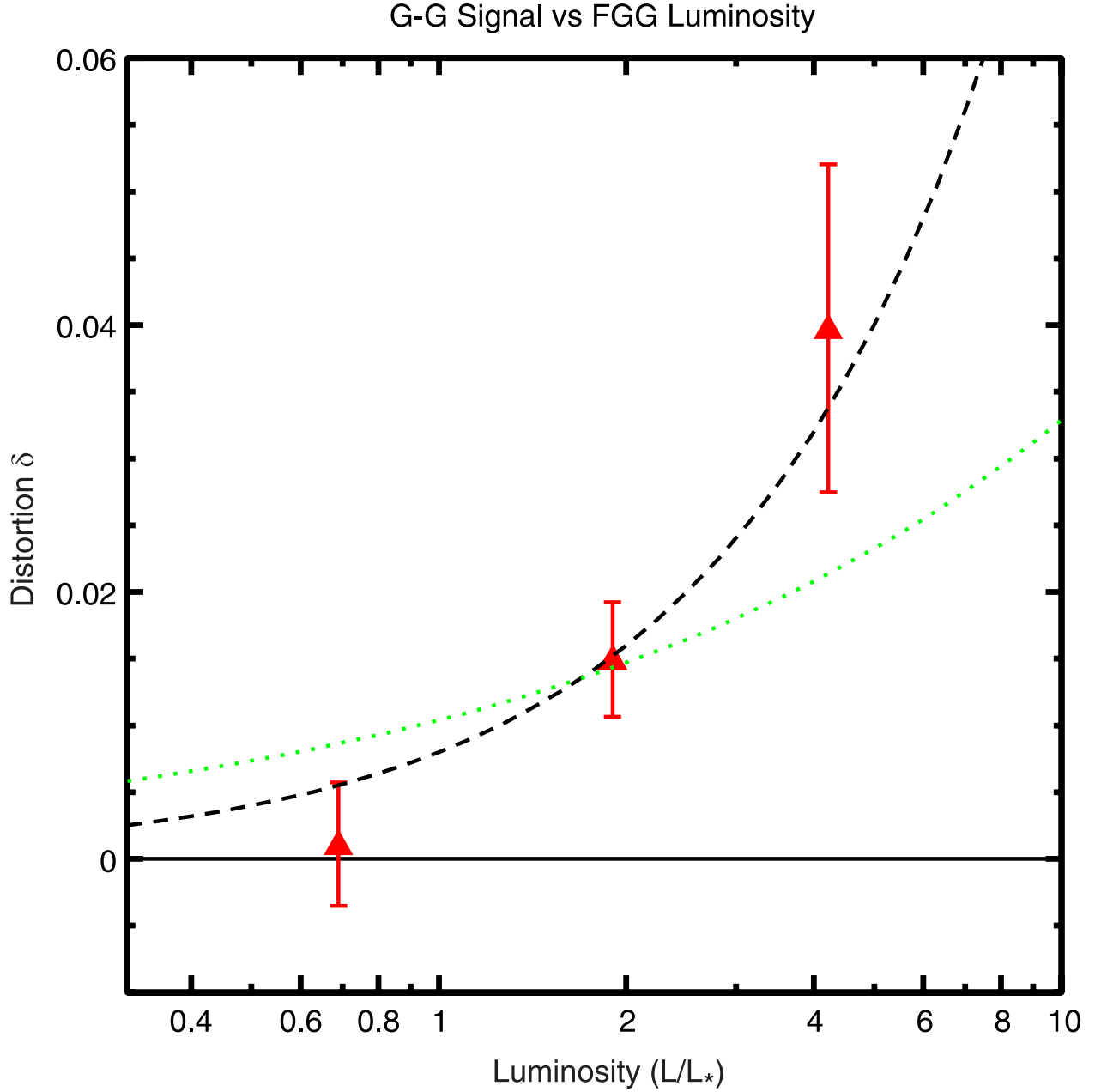


Fig. 3.— The measured distortion  $\delta$  (at  $R = 60h^{-1}$  kpc) is plotted for three bins of foreground galaxy luminosity  $L$ . Dependence of distortion (and hence mass) upon  $L$  is clearly detected. The dashed line is the best-fit mass-traces-light model ( $M \propto L$ ), which fits the data well; the dotted line is the best-fit Faber-Jackson model ( $M \propto L^{0.5}$ ), which is only marginally acceptable.

## 4. Comparison to Other Determinations

### 4.1. Comparison with Other Galaxy-Galaxy Lensing Estimates

We place our result in context first with previous measures of galaxy-galaxy lensing. Most previous works were parameterized by the halo circular velocity of an  $L_*$  galaxy in the isothermal portion of the halo, which we have called  $v_*$ . Our measure of  $\delta_*$  gives 1-sigma limits on  $v_*$  of

$$v_* = \begin{cases} 176 \pm 22 \text{ km s}^{-1} & (\beta = 0.5) \\ 164 \pm 20 \text{ km s}^{-1} & (\beta = 1.0). \end{cases} \quad (26)$$

This is in reasonable agreement with the determinations of Brainerd, Blandford, & Smail (1996) ( $v_* = 220 \pm 80 \text{ km s}^{-1}$ , 90% CL), Hudson *et al.* (1998) ( $v_* = 210 \pm 40 \text{ km s}^{-1}$ ) and of F00 (200–280  $\text{km s}^{-1}$ , 95% CL), given that the disparate definitions of  $L_*$  have been used (the LCRS value is on the low side). We emphasize, however, that ours is the first determination of this quantity to actually measure the luminosities of the foreground galaxies to give a result which is not heavily dependent upon assumptions about the luminosity and redshift distributions of the galaxy populations.

### 4.2. Comparison with Other Dynamical Estimates

Zaritsky & White (1994) use the satellite galaxy data to constrain the mass  $M_{200}$  enclosed within a  $200h^{-1}$  kpc sphere of their typical spiral to be  $1.1\text{--}2.0 \times 10^{12} h^{-1} M_\odot$ . Our results imply a mass within  $200h^{-1}$  kpc of  $(1.25 \pm 0.25)(L/L_*) \times 10^{12} h^{-1} M_\odot$  for  $\beta = 1$ , or  $(1.44 \pm 0.36)\sqrt{L/L_*} \times 10^{12} h^{-1} M_\odot$  for  $\beta = 0.5$ . There is general agreement, but a more specific comparison is not possible because Zaritsky & White find no dependence of mass upon primary luminosity ( $\beta \approx 0$  in our terminology) while we find a relatively strong dependence ( $\beta \geq 0.5$ ).

### 4.3. Comparison to the Tully-Fisher Relation

It is of interest to compare the circular velocity of the halo to the circular velocity of the gaseous disk. Tully *et al.* (1998) present a calibration of the Tully-Fisher relation (TFR) for Ursa Major and Pisces cluster spirals in the  $R$  band. The slope of their  $R$ -band TFR is equivalent to  $\beta = 0.62$ . But they also find that the extinction is stronger in brighter galaxies, and the LCRS magnitudes are not corrected for extinction, so the mass-luminosity relation in the LCRS data would appear somewhat shallower,  $\beta = 0.58$ , for a typical galaxy at  $\sim 60^\circ$  inclination. For this value of  $\beta$ , the lensing data suggest a circular velocity  $v_* = 176 \pm 22 \text{ km s}^{-1}$  at an effective radius of  $\approx 60h^{-1}$  kpc. The TFR calibration yields a disk circular velocity of  $160 \text{ km s}^{-1}$  for a typically-inclined spiral at the LCRS value of  $L_*$ . This consistency suggests that the isothermal mass profile observed at  $\sim 10h^{-1}$  kpc in the disk matches fairly well onto the halo profile at  $\sim 100h^{-1}$  kpc. Even if galaxies have perfect isothermal profiles, we might expect the lensing  $v_*$  to be slightly higher than the TFR value (for late-type spirals) because of the inclusion of early types in the lensing foreground sample.

## 5. Conclusions

The relations between galaxy luminosity and halo mass determined herein provide basic constraints to models of galaxy formation and evolution. We find, perhaps surprisingly, that the halo circular velocity at  $60\text{--}100h^{-1}$  kpc radii are similar to the disk circular velocities measured at  $\lesssim 10h^{-1}$  kpc, extending the “disk-halo conspiracy” to larger radii than previously known. There are hints in the data, however, that this conspiracy breaks down in the sense that halo masses vary more sharply with galaxy luminosity than would be indicated by the Tully-Fisher or Faber-Jackson relations.

The matter density  $\Omega_m$  has been measured by many methods in the past, and there is a currently fashionable consensus that  $\Omega_m \approx 0.3$ . Our results (Equation [25]) are in agreement with this consensus given that our method produces only a lower limit. Our limits are, however, close to the consensus value, especially if  $\beta \approx 0.5$ . Our lower limit on  $\Omega$  is determined by a direct inventory of the matter in the Universe; the only untested assumption is that the formula for gravitational deflection of light can be extrapolated from Solar-System scale (where it has been verified) to galactic scales. Other determinations of  $\Omega$  rely upon assumptions about the nature of our Universe. Agreement between our direct inventory and these other measures serves as valuable and unique verification that these assumptions—often fundamental to our current view of cosmology—are correct.

The more precise estimates of  $\Omega_m$  include the following: Dynamical studies of galaxy clusters, combined with the assumption that the  $M/L$  ratio for clusters is universal, yield  $\Omega_m = 0.24^{+0.05}_{-0.09}$  (Carlberg *et al.* 1996). Another cluster-based means to  $\Omega$  is to measure the fraction  $f_b$  of the cluster matter that is baryonic, assume that the cluster  $f_b$  is universal, and then use the baryon density  $\Omega_b$  from Big Bang nucleosynthesis to estimate  $\Omega_m = \Omega_b/f_b$ . Mohr, Mathiesen, & Evrard (1999) conclude that  $\Omega_m < 0.30 \pm 0.04$  (for  $h = 0.7 \pm 0.1$ ).

Other estimates of  $\Omega$  measure its effects upon global geometry or the growth rate of fluctuations in the Universe. In the former category, the combination of high-redshift supernovae measurements and the location of the cosmic background Doppler peaks measured by MAXIMA-1 constrain  $0.25 < \Omega_m < 0.50$  at 95% CL (Balbi *et al.* 2000). Peculiar velocity studies determine the parameter  $\beta_I \approx \Omega^{0.6}/b$  to be  $\approx 0.5 \pm 0.05$  (Strauss & Willick 1998), with  $b$  a galaxy bias parameter. Taking  $b \approx 1$  gives a value of  $\Omega \approx 0.3$ , again slightly above our halo density. Conversely our lower limit on  $\Omega$  implies a bias parameter for IRAS galaxies  $b \gtrsim 0.7$ .

Thus our results may be taken as independent evidence that these underlying assumptions are correct: cluster  $M/L$  and baryon fractions can be taken as representative; general relativity does properly describe the geometry of the Universe to  $z \approx 1000$  given our directly measured matter content; and large-scale motions are consistent with the predictions of gravitational instability.

Conversely, we may take the  $\Omega_m \approx 0.3$  value as truth and conclude from these lensing results that most of the matter in the Universe is indeed contained within  $260h^{-1}$  kpc of normal galaxies.

This implies that galaxies missed by the LCRS survey—*e.g.* low-surface-brightness galaxies or exotic dark galaxies—cannot be the dominant reservoirs of mass in the Universe. Likewise there cannot be a dominant matter component which is not clustered around galaxies. Most of the mass in the Universe appears to have been located, though of course its material nature remains unknown.

The accuracy of our results is currently limited by the number of foreground/background pairs in our survey. This will be remedied in dramatic fashion by the full Sloan Digital Sky Survey, which will obtain imaging to  $r' < 22$  around roughly *three orders of magnitude* more foreground galaxies than used in this study with a concomitant increase in the number of pairs. This will allow for non-parametric mapping of the shear profile as a function of radius, galaxy luminosity, and galaxy type, with much lower noise than in our LCRS lensing survey. This weak lensing information will be unique in unveiling the relation between the various classes of galaxies and the dark halos in which they reside. With the random errors reduced, closer attention will have to be paid to some of the  $\lesssim 5\%$  corrections we have ignored (as in F00), but these are tractable.

Our estimates of  $M_*$  and  $\Omega$  are lower bounds since the profile of the halo has not yet been determined beyond  $260h^{-1}$  kpc. Beyond this radius it becomes inappropriate to speak of “the halo” of a galaxy, as the mass profile of a given galaxy becomes inseparable from the mass associated with neighboring galaxies. More stringent limits on  $\Omega$  will thus require a more elaborate formalism for describing the effects of galaxy correlations upon the weak lensing measurements.

This work was supported by grant AST-9624592 from the National Science Foundation. We gratefully acknowledge the assistance of J. A. Tyson and David Wittman with the construction and operation of the BTC camera and their contributions to the data pipeline; Tim McKay and Erin Sheldon for continued discussions of SDSS lensing results; and the staff of CTIO for their enthusiastic support of the BTC observations.

## REFERENCES

- Balbi, A. *et al.* 2000, astro-ph/0005124
- Bernstein, G. M., Jarvis, R. M., Fischer, P., & Smith, D. R., 2000 (in preparation)
- Bertin, E., & Arnouts, S. 1996 A&A, 117, 393
- Brainerd, T.G., Blandford, R.D., & Smail, I. 1996, ApJ, 466, 623
- Carlberg, R. G. *et al.* 1996, ApJ, 462, 32
- Cohen, J. G. *et al.* 2000, ApJ (in press) astro-ph/9912048
- Crampton, D., Le Fèvre, O., Lilly, S.J., & Hammer, F. 1995, ApJ, 455, 96

- Dell’Antonio, I.P. & Tyson, J.A. 1996, ApJ, 473, L17
- Fischer, P. & Tyson, J. A. 1997, AJ, 114, 14
- Fischer, P. *et al.*2000 , ApJ (in press) astro-ph/9912119 (F00)
- Griffiths, R.E., Casertano, S., Im, M., & Ratnatunga, K.U. 1996, MNRAS, 282, 1195
- Hudson, M.J., Gwyn, S.D.J., Dahle, H., & Kaiser, N., 1998, ApJ, 503, 531
- Kaiser, N., Squires, G., & Broadhurst, T. 1995, ApJ, 449 460
- Landolt, A.U. 1992, AJ, 104, 340
- Lin, H., Kirshner, R. P., Sackett, S.A., Landy, S. D., Oemler, A., Tucker, D. L., & Schechter, P. L. 1996, ApJ, 464, 60
- Mohr, J. J., Mathiesen, B., & Evrard, A. 1999, ApJ, 517, 627
- Sackett, S. A., Landy, S. D., Oemler, A., Tucker, D. L., Lin, H., Kirshner, R.P., & Schechter, P. L. 1996, ApJ, 470, 172
- Smith, D. R. 2000, PhD Thesis, University of Michigan
- Stebbins, A., McKay, T., & Frieman, J. 1996, in “IAU 173: Astrophysical Applications of Gravitational Lensing,” eds. C. S. Kochanek & J. N. Hewitt (Kluwer), 75
- Strauss, M. & Willick, S. 1998, ApJ, 507, 64
- Tully, R. B. *et al.*1998, AJ, 115, 2264
- Tyson, J.A., 1988, AJ, 96, 1
- Tyson, J.A, Valdes, F., Jarvis, J.F., & Mills, A.P. 1984, ApJ, 281, L59
- Wittman, D.M., Tyson, J.A., Dell’Antonio, I.P., Bernstein, G.M., & Smith, D.R. 1998, Proc. SPIE3355, 626-634
- Zaritsky, D. & White, S.D.M., 1994, ApJ, 435, 599
- Zaritsky, D., Smith, R., Frenk, C., & White, S.D.M., 1997, ApJ, 478, 39